Development of Multianalyte Sensor Arrays Composed of Chemically Derivatized Polymeric Microspheres Localized in Micromachined Cavities

Adrian Goodey,[†] John J. Lavigne,[†] Steve M. Savoy,[†] Marc D. Rodriguez,[†] Theodore Curey,[†] Andrew Tsao,[†] Glen Simmons,[†] John Wright,[†] Seung-Jin Yoo,[‡] Youngsoo Sohn,[‡] Eric V. Anslyn,[†] Jason B. Shear,[†,§] Dean P. Neikirk,[‡] and John T. McDevitt*[,‡,||,#]

Contribution from the Department of Chemistry & Biochemistry, Department of Electrical & Computer Engineering, Institute for Cellular & Molecular Biology, Center for Nanostructured Materials, and Texas Materials Institute, The University of Texas at Austin, Austin, Texas 78712

Received September 11, 2000

Abstract: The development of a chip-based sensor array composed of individually addressable polystyrene−poly(ethylene glycol) and agarose microspheres has been demonstrated. The microspheres are selectively arranged in micromachined cavities localized on silicon wafers. These cavities are created with an anisotropic etch and serve as miniaturized reaction vessels and analysis chambers. A single drop of fluid provides sufficient analysis media to complete ∼100 assays in these microetch pits. The cavities possess pyramidal pit shapes with trans-wafer openings that allows for both fluid flow through the microreactors/analysis chambers and optical access to the chemically sensitive microspheres. Identification and quantitation of analytes occurs via colorimetric and fluorescence changes to receptor and indicator molecules that are covalently attached to termination sites on the polymeric microspheres. Spectral data are extracted from the array efficiently using a charge-coupled device allowing for the near-real-time digital analysis of complex fluids. The power and utility of this new microbead array detection methodology is demonstrated here for the analysis of complex fluids containing a variety of important classes of analytes including acids, bases, metal cations, metabolic cofactors, and antibody reagents.

Introduction

A number of novel chemical sensing strategies have been developed that utilize polymer-supported indicator systems.[1−14] Historically, one of the most commonly employed techniques has exploited colloidal polymer microspheres for latex agglutination tests (LATs) in clinical analyses. Commercially available LATs for more than 60 analytes[15] are used routinely for the detection of infectious disease, illegal drugs, and even early pregnancy tests. The vast majority of these types of sensors operate on the principle of agglutination of latex particles (polymer microspheres),[16] which occurs when the antibody-derivatized microspheres become effectively "cross-linked" by a foreign antigen. The process results in the microspheres becoming attached to, or unable to pass through, a filter. The dye-doped microspheres are then detected colorimetrically upon removal of the antigen-carrying solution. However, LATs cannot be utilized for multiple analyte detection schemes as the nature of the response intrinsically depends on a cooperative effect of the entire collection of microspheres.

More recently, exciting new developments have been made that broaden the scope of polymer-supported sensor methodologies, to create sensor arrays that function as "electronic noses".[4,17−19] Like the mammalian sense of smell, these arrays can be used to assay for a variety of vapor-phase analytes. For the artificial nose systems prepared to date, a variety of detection

* To whom correspondence should be addressed. E-mail: mcdevitt@mail.utexas.edu.
[†] Department of Chemistry & Biochemistry.
[‡] Department of Electrical & Computer Engineering.
[§] Institute for Cellular & Molecular Biology.
[||] Texas Materials Institute.
[#] Center for Nanostructured Materials.

(1) Amrani, M. E. H.; Ibrahim, M. S.; Persaud, K. C. *Mater. Sci. Eng. C* **1994**, *1*, 17−22.
(2) Dafu, C.; Qiang, C.; Jinghong, H.; Jinge, C.; Yating, L.; Zemin, Z. *Sens. Actuators, B* **1993**, *12*, 29−32.
(3) Denizli, A.; Kokturk, G.; Salih, B.; Kozluca, A.; Piskin, E. *J. Appl. Polym. Sci.* **1997**, *63*, 27−33.
(4) Dickinson, T. A.; White, J.; Kauer, J. S.; Walt, D. R. *Nature* **1996**, *382*, 697−700.
(5) Dickinson, T. A.; Michael, K. L.; Kauer, J. S.; Walt, D. R. *Anal. Chem.* **1999**, *71*, 2192−2198.
(6) Lavigne, J. J.; Savoy, S.; Clevenger, M. B.; Ritchie, J. E.; McDoniel, B.; Yoo, S. J.; Anslyn, E. V.; McDevitt, J. T.; Shear, J. B.; Neikirk, D. *J. Am. Chem. Soc.* **1998**, *120*, 6429−6430.
(7) Walt, D. R. *Science* **2000**, *287*, 451−452.
(8) Healey, B. G.; Foran, S. E.; Walt, D. R. *Science* **1995**, *269*, 1078−1080.
(9) Golunski, W.; Hypszer, R.; Plucinski, J. *Proc. SPIE-Int. Soc. Opt. Eng.* **1989**, *1085*, 470−472.
(10) Kirkbright, G. F.; Narayanaswamy, R.; Welti, N. A. *Analyst* **1984**, *109*, 15−17.
(11) Peterson, J. I.; Goldstein, S. R.; Fitzgerald, R. V.; Buckhold, D. K. *Anal. Chem.* **1980**, *52*, 864−869.
(12) Rouhi, A. M. *Chem. Eng. News* **1997**, *75* (May 12), 41−45.
(13) Schild, D., Ed. *Chemosensory Information Processing*; Springer: Berlin, 1990.
(14) Arenkov, P.; Kukhtin, A.; Gemmell, A.; Voloshchuk, S.; Chupeeva, V.; Mirzabekov, A. *Anal. Biochem.* **2000**, *278*, 123−131.
(15) Bangs, L. B. *Pure Appl. Chem.* **1996**, *68*, 1873−1879.
(16) Shahar, M.; Meshulam, H.; Margel, S. *J. Polym. Sci.* **1986**, *24*, 203−213.
(17) Lewis, N. S.; Lonergan, M. C.; Severin, E. J.; Doleman, B. J.; Grubbs, R. H. *Proc. SPIE-Int. Soc. Opt. Eng.* **1997**, *3079*, 660−670.
(18) Logergan, M. C.; Severin, E. J.; Doleman, B. J.; Beaber, S. A.; Grubbs, R. H.; Lewis, N. S. *Chem. Mater.* **1996**, *8*, 2298.
(19) Walt, D. R.; Dickinson, T. A.; Healey, B. G.; Kauer, J. S.; White, J. *Proc. SPIE-Int. Soc. Opt. Eng.* **1995**, *2508*, 111−116.

10.1021/ja003341l CCC: $20.00
Published on Web 02/21/2001

modalities have been used successfully for the classification, identification, and quantitation of vapor-phase reagents. These methods exploit conductive polymers,[20] carbon black-insulating polymer composites,[21] dye-doped polymer matrixes,[4,22] modified tin oxide sensors,[23,24] quartz crystal microbalances,[25] and surface acoustic wave transducers coated with molecular reagents.[26−29] In the recent past, a chemoselective colorimetric vapor sensor array has emerged.[30] The sensor is based upon vapor-phase attachment of volatile ligands to immobilized metalloporphyrins, yielding detectable spectral changes.

While these prior works demonstrate the utility of array systems for studying the chemical composition of complex vapors, it is clear that these systems possess a number of limitations. One of the most significant deficiencies is that these structures, in their current forms, are limited to multicomponent analyses completed within the vapor phase. For many important medical, process control, environmental, food safety, and food/beverage processing applications, the identification of analytes that are difficult to volatilize without decomposition is essential. For these areas, the need for a chemically diverse, solution-phase multianalyte detection system is acute. Here the challenges associated with distinguishing between subtle differences in common electrolytes (Na^+ vs K^+ and Mg^{2+} vs Ca^{2+}), small differences in acidity (citric acid vs lactic acid), slight changes in protein structures (influenza A vs influenza B), and complex sugar isomers (glucose vs galactose) makes the development of chemically diverse solution multianalyte detection arrays a very complex issue. These problems are exacerbated somewhat by interactions that occur within the liquid media where solvent−solute associations can be quite strong. To prepare chemically diverse liquid-phase multianalyte detection schemes, it is expected that a significant amount of effort will be needed for the identification of the appropriate receptor and signaling reagents. Fortunately, the recent advances in the areas of molecular recognition, enzymology, immunology, and molecular biology enable the elaboration of molecular assemblies selective toward binding specific analyte species. However, a significant challenge now exists relative to the definition of an array format and associated detection methodology that can be used in conjunction with these various receptor groups for the assay of multicomponent fluids.

To date there have been a number of interesting initial reports of array methodologies suitable for fluid analyses. These approaches include acoustic wave devices,[31,32] microelectrodes,[33−35] arrays based on conducting polymers,[36] polymerized crystalline colloidal arrays (PCCA),[37] and fiber optic-based sensors.[22,38−40] Moreover, lipid membranes used in combination within electrodes have found utility in mimicking some of the functionality of mammalian taste bud cells.[39,41−47]

Both the senses of taste and smell are chemically based, making their adaptation for sophisticated chemical and biological analyses highly desirable. It is generally assumed that the primary process of chemoreception in the mammalian olfactory system takes place at the cell membrane of these sensory neurons.[48] Like the sense of smell, the mammalian sense of taste occurs as a result of complex chemical analyses that are completed in a parallel fashion at a series of chemically active sites (taste buds). These taste buds are located within depressions in the tongue where the molecular and ionic analytes become restricted to allow time for their identification.[49,50] Here, the five primary tastes are sensed: sweet (carbohydrate based), sour (acidity), salty (ionic), umami (savory), and bitter (quinine and other alkaloids). In nature, these five taste categories are used to analyze the foods being consumed. Combining the magnitude of these five signals, along with information derived from the nose, creates a pattern that is distinctive for each tastant.

Previously, we reported the conceptual and experimental development of a chip-based microsphere array platform suitable for the digital analysis of complex fluids.[6] These "*electronic taste*" chips have the potential to mimic many of the features exhibited by the human sense of taste. That is, multianalyte mixtures can be analyzed and intelligent decisions related to the chemical composition of solution-phase samples can be made rapidly and accurately with this detection modality. Since these initial reports, we have expanded the utility of the chip-based microsphere sensor array by increasing in a dramatic way the analyte detection diversity. Moreover, we have created and automated a "total analysis system" that is presented here for the first time to be capable of the analysis of pH, metal cations, sugars, and antibodies within complex fluids such as beverages, and biological samples. This instrumentation includes an optical microscope station suitable for collection of absorbance and fluorescence signals at multiple sites, a chip holder, and a fluid delivery system. All components have been integrated into a single functional laboratory prototype system. Furthermore, the

(20) Freund, M. S.; Lewis, N. S. *Proc. Natl. Acad. Sci. U.S.A.* **1995**, *92*, 2652−2656.
(21) Lonergan, M. C.; Severin, E. J.; Doleman, B. J.; Beaber, S. A.; Grubb, R. H.; Lewis, N. S. *Chem. Mater.* **1996**, *8*, 2298−2312.
(22) Walt, D. R. *Acc. Chem. Res.* **1998**, *31*, 267−278.
(23) Heilig, A.; Barsan, N.; Weimar, U.; Schweizer-Berberich, M.; Gardner, J. W.; Gopel, W. *Sens. Actuators, B* **1997**, *43*, 45−51.
(24) Gardner, J. W.; Shurmer, H. V.; Tan, T. T. *Sens. Actuators, B* **1992**, *6*, 71−75.
(25) Brunick, J. A. J.; Di Natale, C.; Bungaro, F.; Davide, F. A. M.; D'Amico, R.; Paolesse, R.; Boschi, T.; Faccio, M.; Ferri, G. *Anal. Chim. Acta* **1996**, *325*, 53−64.
(26) Crooks, R. M.; Ricco, A. J. *Acc. Chem. Res.* **1998**, *31*, 219−227.
(27) Grate, J. W.; Abraham, M. H. *Sens. Actuator, B* **1991**, *3*, 85−111.
(28) Nakamoto, T.; Fukunishi, K.; Moriizumi, T. *Sens. Actuators, B* **1990**, *1*, 473.
(29) Nakamoto, T.; Fukuda, A.; Moriizumi, T. *Sens. Actuators, B* **1993**, *10*, 85.
(30) Rakow, N. A.; Suslick, K. S. *Nature* **2000**, *406*, 710−713.
(31) Chen, K.; Wang, D. *IEEE* **1998**, *1*, 619−624.
(32) Nakamoto, T. *Acoust. Imaging* **1989**, *17*, 619−626.
(33) Lauks, I. R. *Acc. Chem. Res.* **1998**, *31*, 317−324.
(34) Amatore, C. A. In *Physical Electrochemistry: Principle, Method and Applications*, 1st ed.; Rubenstein, I., Ed.; Marcel Dekker: New York, 1995; pp 131−208.
(35) Wightman, R. M.; Wipf, D. O. In *Electroanalytical Chemistry*; Bard, A. J., Ed.; Marcel Dekker: New York, 1989; Vol. 15, pp 267−353.
(36) Sangodkar, H.; Sukeerthi, S.; Srinivasa, R. S.; Lal, R.; Contractor, A. Q. *Anal. Chem.* **1996**, *68*, 779−783.
(37) Holtz, J. H.; Holtz, J. S. W.; Munro, C. H.; Asher, S. A. *Anal. Chem.* **1998**, *70*, 780−791.
(38) Healey, B. G.; Chadra, S.; Walt, D. R.; Milanovich, F. P.; Richards, J.; Brown, S. *Proc. SPIE-Int. Soc. Opt. Eng.* **1994**, *2360*, 10110−10112.
(39) Walt, D. *CHEMTECH* **1992**, *22* (Nov), 658−663.
(40) Michael, K. L.; Taylor, L. C.; Schultz, S. L.; Szurdoki, F.; Walt, D. R. *Proc. SPIE-Int. Soc. Opt. Eng.* **1998**, *3270*, 34−41.
(41) Hayashi, K.; Yamanaka, M.; Toko, K.; Yamafuji, K. *Sens. Actuators, B* **1990**, *2*, 205−213.
(42) Lenzmann, F.; Li, K.; Kitai, A. H.; Stover, H. D. H. *Chem. Mater.* **1994**, *6*, 156−159.
(43) Pantano, P.; Walt, D. R. *Anal. Chem.* **1995**, *67*, 481A−487A.
(44) Healey, B. G.; Walt, D. R. *Anal. Chem.* **1995**, *67*, 4471−4475.
(45) Pantano, P.; Walt, D. R. *Chem. Mater.* **1996**, *8*, 2832−2835.
(46) Healey, B. G.; Walt, D. R. *Anal. Chem.* **1997**, *69*, 2213−2216.
(47) Dickinson, T. A.; Walt, D. R.; White, J.; Kauer, J. S. *Anal. Chem.* **1997**, *69*, 3413−3418.
(48) Schleppnik, A. A., Ed. *Structure Recognition as a Peripheral Process in Odor*; American Chemical Society: Washington, DC, 1981; Vol. 148.
(49) Schmale, H.; Ahlers, C.; Blaker, M.; Kock, K.; Spielman, A. I. In *The Molecular Basis of Small and Taste Transduction*; Chadwick, D., Marsh, J., Goode, J., Eds.; John Wiley & Sons: Chichester, U.K., 1993; pp 167−185.
(50) Getchell, T. V. *Physiol. Rev.* **1990**, *66*, 772.

instrumentation system has been refined to enable the automated collection of optical data recorded at multiple microsphere sites while the local chemistry/biochemistry thereat is altered. With this new instrumentation, reproducibility, reversibility, concentration thresholds, and response times have now been measured for both static and flow-based experiments. In this paper, we summarize the new developments and describe the power/utility of this new microsphere array detection methodology in the context of the analysis of complex fluids containing various acidities, metal cations, sugars, and antibody contents.

Experimental Section

Materials. Polystyrene−poly(ethylene glycol) (PS−PEG) graft copolymer microspheres (~130 μm in diameter when dry and ~230 μm when hydrated) were purchased from Novabiochem. Normal amine activation substitution levels for these beads were between 0.2 and 0.4 mmol/g. Commercial-grade reagents were purchased from Aldrich and used without further purification except as indicated below. Fluorescein isothiocyanate was purchased from Molecular Probes. All solvents were purchased from EM Science, and those used for solid-phase syntheses were dried over molecular sieves. Methanol was distilled from magnesium turnings.

Immunoassays were performed using carbonyl diimidazole (CDI) activated Trisacryl GF-2000 available from Pierce Chemical (Rockford, IL). The particle size for this support ranged between 40 and 80 μm. The reported CDI activation level was >50 μmol/mL gel. Viral antigen and monoclonal antibody reagents were purchased from Biodesign International (Kennebunk, ME). Rhodamine and Cy2[51]-conjugated goat anti-mouse antibody was purchased from Jackson ImmunoResearch Laboratories, Inc. (West Grove, PA). Antigen and antibody reagents were aliquoted and stored at 2−8 °C for short term and at −20 °C for long term. Goat anti-mouse antibody was diluted with glycerol (50%)/water (50%) and stored at −20 °C.

Agarose beads (6% cross-linked) used for the enzyme-based studies were purchased from XC Bead Corp. (Lowell, MA). The beads were glyoxal activated (20 μmol of activation sites/mL) and were stored in sodium azide solution. Agarose bead sizes ranged from 250 to 350 μm.

General Procedures. All final functionalized PS−PEG copolymer microsphere batches (resin) were dried under high vacuum for at least 12 h. The resin was washed thoroughly before and after each coupling reaction on the solid phase using a rotary evaporator motor to tumble the reaction vessel in an oblong fashion (shaking), for a specified period of time (i.e., the "1 × 1" notation refers to one wash for 1 min before the solvent was drained).

(a) Solid-Phase Peptide Synthesis Forming an Amide Linkage between the Indicator and the Resin (i.e., Alizarin Complexone and o-Cresolphthalein Complexone).[52−56] Amino-terminated polystyrene−poly(ethylene glycol) graft copolymer resin (0.20 g, 0.29 mmol/g, 0.058 mmol) was placed in a solid-phase reaction vessel and washed with 1 × 1 min dichloromethane, 2 × 5 min *N*,*N*-dimethylformamide (DMF), and 2 × 2 min dichloromethane. While the resin was being washed, an oven-dried round-bottom flask was charged with dicyclohexylcarbodiimide (DCC) (0.059 g, 0.29 mmol, 5.0 equiv) and hydroxybenzotriazole (HOBt) (0.039 g, 0.29 mmol, 5.0 equiv) in 8 mL of DMF and cooled in an ice bath. To this mixture, alizarin complexone (0.20 g, 0.29 mmol, 5.0 equiv) was added and the solution stirred at 0 °C for 30 min. After the resin washes were completed, this solution was filtered and added to the resin. The heterogeneous system was allowed to shake for 2−15 h at 25 °C. At the end of this time, the coupling solution was removed and the resin was washed with 2 × 2 min DMF, 1 × 2 min dichloromethane, 1 × 2 min methanol, 1 × 5 min DMF, and 1 × 1 min dichloromethane. A small portion of this resin was then subjected to a quantitative ninhydrin (Kaiser) test to assay for the presence of primary amines, using Merrifield's quantitative procedures.[57,58] Various indicator substitution levels were used as required for the desired assays.

Other dyes such as xylenol orange (Sigma), calconcarboxylic acid (Aldrich), and thymolphthalexon (Aldrich) were conjugated to the resin beads using similar protocols as described above.

(b) Acetylated Resin. Prewashed resin (0.10 g, 0.29 mmol/g, 0.029 mmol) was treated with acetic anhydride (1.5 mL, 16 mmol, 550 equiv) and triethylamine (0.034 g, 7.2 mmol, 250 equiv) in 5 mL od dichloromethane. After 30 min of shaking at 25 °C, the reaction mixture was removed and the resin was washed (as described above). A ninhydrin test produced a negative result.

(c) Solid-Phase Peptide Synthesis Forming a Thiourea Linkage between the Indicator (Fluorescein) and the Resin. Once the resin (0.075 g, 0.30 mmol/g, 0.022 mmol) had been completely washed, fluorescein isothiocyanate (0.034 g, 0.087 mmol, 4.0 equiv) in 5 mL of dichloromethane and 5 mL of DMF was added to it. Two different levels of dye loading were created to service the specific needs of the colorimetric and fluorescence-based measurements. If the resin was to be used for colorimetric studies, it was allowed to shake in an oven at 55 °C for 1−5 days. The subsequent workup of washes was followed as previously mentioned. If a positive ninhydrin test was obtained, the resin was resubmitted to the reaction conditions until ninhydrin gave a negative result. Resin designated for fluorescence studies was shaken at 25 °C only for 1−3 days as lower dye loading was needed. A quantitative ninhydrin test was then performed to assess the level of substitution. A low loading volume was required to minimize fluorescence self-quenching.

(d) Viral Immunoassays. Hepatitis B surface antigen (HbsAg) was coupled to the CDI-activated Trisacryl support in the following manner: 20 μL of a 50% (by volume) bead slurry was pipetted into a 0.6-mL microcentifuge tube. The number of moles of activated CDI sites per milliliter of bead slurry was determined and reacted with HBsAg in a 1:3000 ratio (1 mol of protein/3000 mol of CDI sites). To the microcentrifuge tube was added 500 μL of a solution of phosphate-buffered saline at pH 8. The resulting reaction mixture was allowed to react overnight at room temperature with shaking. Similar procedures were performed with HIV gp 41/120 and influenza A antigens.

(e) Immobilized Enzyme Sensors. Diaphorase was immobilized onto porous cross-linked agarose beads (XC Bead Corp., Lowell, MA). The beads were purchased preactivated with glyoxal groups. In a standard procedure for enzyme immobilization, about 2 mg of lyophilized diaphorase was dissolved into a 1.00-mL solution of 200 mM phosphate buffer at pH 7.00. To a 1.5-mL Eppendorf tube was added 100 μL of fresh beads and the supernatant was removed with a pipet. To the beads was added 500 μL of 200 mM phosphate buffer (pH 7.00). A 50-μL aliquot of the diaphorase suspension was combined to the bead slurry, and finally, 20 μL of a 0.75 mM solution of sodium cyanoborohydride was added to the mixture. The resulting sample was then shaken at the lowest speed on a Vortex Genie overnight. The supernatant was removed the next day, and the beads were washed with 200 mM phosphate buffer (pH 7.00) twice before use.

Fabrication of the Microbead Arrays. (a) Micromachined Bead Arrays. Individual microspheres were placed into chemically etched microcavities patterned in a square array on 4-in. single crystal (100) double polished silicon wafers (~220 μm thick) using a micromanipulator on an *x*−*y*−*z* translator. The cavities were prepared using bulk KOH anisotropic etching of the silicon substrate. To mask the substrate during the KOH etch, a silicon nitride layer was prepared using a low-pressure chemical vapor deposition (LPCVD) technique. Removal of the mask layer from one side of the silicon substrate was carried out by protecting the other side with photoresist and plasma

(51) *BioDirectory 2000, Amersham Pharmacia Biotech 2000 Catalog*; Amersham Pharmacia Biotech: Piscataway, NJ, 2000.
(52) Merrifield, R. B. *J. Am. Chem. Soc.* **1963**, *85*, 2149−2154.
(53) Stewart, J. M.; Young, J. D. *Solid-Phase Peptide Synthesis*; W. H. Freeman: San Francisco, 1969.
(54) Jones, J. *The Chemical Synthesis of Peptides*; Clarendon Press: Oxford, U.K., 1991.
(55) Bodanszky, M. *Principles of Peptide Synthesis*, 2nd ed.; Springer-Verlag: Berlin, 1993.
(56) Basava, C.; Anantharamaiah, G. M. In *Peptides: Design, Synthesis, and Biological Activity*; Basava, C., Anantharamaiah, G. M., Eds.; Birkhauser: Boston, 1994.
(57) Kaiser, E.; Colescott, R. L.; Bossinger, C. D.; Cook, P. I. *Anal. Biochem.* **1970**, *34*, 595−598.
(58) Sarin, V. K.; Kent, S. B. H.; Tam, J. P.; Merrifield, R. B. *Anal. Biochem.* **1981**, *20*, 147−157.

etching (CF_4 and O_2 at 100 W) the Si_3N_4 layer. The silicon substrate was etched anisotropically[59−62] using a 40% KOH solution (Transene silicon etchant PSE-200). The etch rate of the (100) silicon was ∼1 μm/min at 100 °C. Successful patterning requires that a highly stable temperature be maintained throughout the etch process. After completion of the KOH etch, the nitride masking layer was completely removed from both sides of the silicon substrate using plasma etching. To improve surface wetting characteristics, the completed device was soaked in 30% H_2O_2 for 15−20 min to form a thin SiO_2 layer on the surface of the silicon.

(b) Fluid Package. Construction of the flow cell began with the machining of two Teflon frames. Drilling a hole through the Teflon allowed for the penetration of the interior of the frame with segments of the fluid delivery tubing. A siloxane polymer casing was then poured around each frame−tubing ensemble. Two different molds were used when the siloxane resin was poured. The mold for the upper layer coated the Teflon with a thin layer of resin and filled in the center of the frame but left a shallow indentation in the center (at the end of the PEEK tubing), which served as a reservoir. The lower mold yielded an almost identical piece, except that it had two concentric indentations: one to hold the chip in place and a second to serve as a reservoir below the array of beads. The chip was then placed between the two siloxane/Teflon layers, and the multilayered structure was held together by an aluminum casing. The resulting assembly was a cell with optical windows above and below the chip and a small exchange volume (∼50 μL) capable of handling flow rates as high as 10 mL/min.

Instrumentation. (a) Fluid Delivery. Solutions were typically introduced into the flow cell using an Amersham Pharmacia Biotech ÄKTA Fast Protein Liquid Chromatograph (FPLC). This instrumentation was used without placement of in-line chromatographic columns and served as a precise, versatile, and programmable pump. The FPLC instrumentation included a number of on-board diagnostic elements that aided in the characterization of the system. The siloxane layers mentioned above were used to hold the chip in place and also provided fluid coupling to the delivery tubing.

Beads within the sensor array were exposed to analytes as solution was pumped into the upper reservoir of the cell, forced down through the wells to the lower reservoir and out through the drain. The cell was designed specifically to force all introduced solution to pass through the wells of the array. The FPLC unit utilized here was able to draw from as many as 16 different solutions and was also equipped with an injection valve and sample loop, allowing for a wide range of fluid samples to be analyzed.

(b) Microscope and CCD Camera. The flow cell sat on the stage of an Olympus SZX12 stereomicroscope. The microscope was outfitted for both top and bottom light illumination. The scope also had a mercury lamp for fluorescence excitation. Removable filter cubes were inserted to control the excitation and emission wavelengths. The array was observed through the microscope optics, and images were captured using an Optronics DEI-750 3-chip charge-coupled device (CCD) (mounted on the microscope) in conjunction with an Integral Technology Flashbus capture card.

(c) Software. Image Pro Plus 4.0 software from Media Cybernetics was used on a Dell Precision 420 workstation to capture and analyze images. Solution introduction, image capture, and data extraction were completed in an automated fashion. The FPLC was controlled by Unicorn 3.0 software (Amersham Pharmacia Biotech).

(d) Total Analysis System. Automated data acquisition and analysis was completed typically as a multistep process. Initially, methods were composed within the FPLC's software. The method was laid out as a time line and controlled the fluid delivery (i.e., flow rate, solution concentration, timing of sample injections, etc.). Similarly, macros within the imaging software were used to control the timing and frequency of data capture. Typically, raw data were in the form of a movie or a sequence of images. After a sequence had been captured, there was a pause in the automation, during which time the user would define specific areas of interest to be analyzed (i.e., the central regions of the beads) and also specify what information was to be extracted (i.e., average red, green, and blue intensities). A macro would then proceed through the sequence of images applying the same areas of interest to each frame and exporting the appropriate information to a preformatted spreadsheet.

Other Instrumentation. The ^1H and ^{13}C NMR spectra were obtained in $CDCl_3$ solvent solution that was used as purchased. Spectra were recorded on a Varian Unity 300 (300 MHz) Instrument. Low- and high-resolution mass spectra were measured with Finnigan TSQ70 and VG analytical ZAB2-E mass spectrometers, respectively. Immunoassay reagent quality control tests were performed on a Molecular Devices SpectraMax Plus UV/visible microplate reader and a Molecular Devices SpectraMax Gemini XS spectrofluorometer microplate reader.

Results and Discussion

The development of a chip-based system suitable for the analysis of complex fluids represents an important new strategy for solution-phase multianalyte detection. Essential for the creation of such an artificial "taste chip" sensory system is the ability to recognize and bind the analytes of interest. To complete multiple analyses in parallel, it is desirable to utilize a chip-based method that benefits from the advantages offered by lithographic procedures such as mass production of identical units, small size, and inexpensive costs. As defined previously,[6] our microbead sensor array platform consists of polymer microspheres immobilized into small voids which are fashioned within Si chips. This etching process removes selective regions of the wafer until the Si (111) crystal faces are exposed. At this point, the etching proceeds much more slowly along this crystallographic direction and thereby results in a series of pyramidal pits whose sides are angled inward at 54.7°, Figure 1A.

The size and location of these pits are controlled by the strategic placement of openings within a silicon nitride etch mask. With the use of the ∼500 μm × ∼500 μm openings on the top Si surface as well as the choice of ∼220-μm-thick Si (100) wafers, it is possible to create 10 × 10 element arrays using ∼5 mm × ∼5 mm size chip fragments. While further reduction in feature size is clearly possible, we have noted that the immediate use of smaller pit sizes complicates the bead placement issue, reduces the accuracy of the single-site optical analyses, and causes problems with the handling/processing of ultrathin wafers. The above stated geometry affords the creation of a 100-site microbead array that can be wetted with a single drop of aqueous fluid. Moreover, this chip landscape yields a density (∼400 sites/cm^2) that is convenient due to its size matching with current generation video chips. With the use of these feature sizes and bead diameters, it is possible to complete analyses using information derived from single beads without the need to combine signals from multiple sites and without the need to identify the sensor type at specific locations. An interesting fiber optic-based alternative that exploits ultrasmall spheres cast within random arrays has been described recently by Walt.[7]

As mentioned above, each of the silicon etch pit areas serves as a microreactor and microanalysis chamber. The chemical selectivity of each site is created through the strategic placement of a derivatized polymeric microsphere, Figure 1B. The physical and chemical characteristics of the polymer microspheres make them an excellent medium for inclusion within multielement sensor arrays. Indeed, a large number of activated beads are

(59) Wolthuis, R.; Mitchell, G.; Saaski, E.; Hartl, J.; Afromowitz, R. *IEEE Trans. Biomed. Eng.* **1991**, *38*, 974−980.
(60) Aratani, K.; French, P. J.; Sarro, P. M.; Poenar, D.; Wolffenbuttel, R. F.; Middlehoek, S. *Sens. Actuators* **1994**, *43A*, 17−23.
(61) Kim, Y.; Neikirk, D. P. *IEEE Photonics Technol. Lett.* **1995**, *7*, 1471−1473.
(62) Han, J.; Neikirk, D. P.; Clevenger, M.; McDevitt, J. T. *Proc. SPIE-Int. Soc. Opt. Eng.* **1996**, *2881*, 171−178.

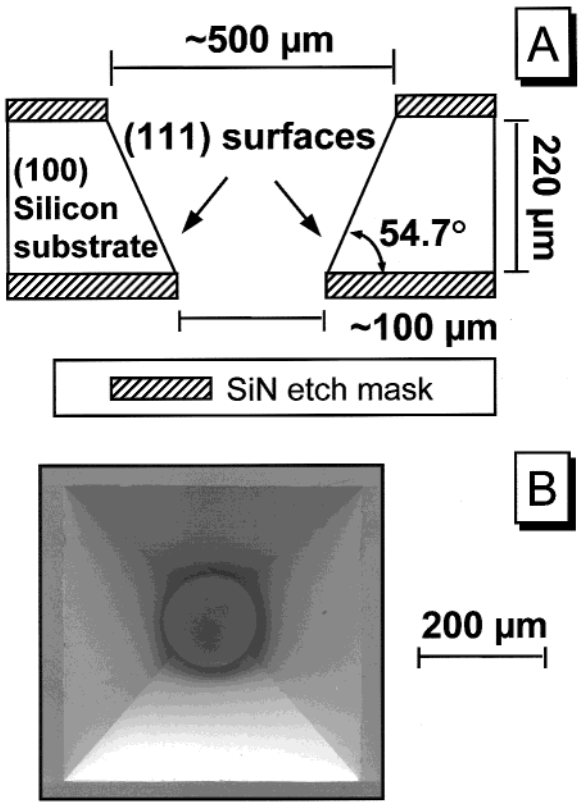

Figure 1. (A) A cross-section diagram displaying the pit region within the silicon wafer that is used to confine the bead sensor elements. Here a square opening (~500 μm × ~500 μm) within the SiN etch mask layer is used in conjunction with an anisotropic etch to expose the silicon (111) surfaces. The resulting pyramidal pits extend through the entire thickness of the wafer, thereby creating square openings (~100 μm × ~100 μm) on the remote side of the chip. These openings both provide optical access to the bead element and serve as a drain for the reaction/analysis chambers. (B) A scanning electron micrograph shows from a top perspective a single well wherein a resin sensor bead is located centrally.

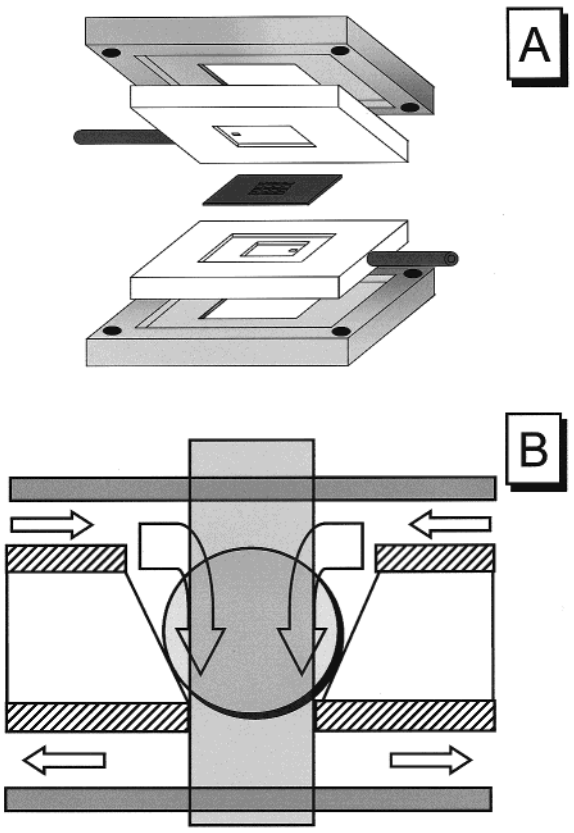

Figure 2. (A) A schematic diagram depicting the fluid package interface. Here two external clamps are used in conjunction with two gasket layers to create a leak-tight enclosure that confines the silicon chip that houses the microbead array. Fluids are introduced into the chip package using flexible, chemically inert plastic tubing. (B) A cross-section schematic shows an expanded view of the fluid delivery method and bead confinement strategy. Fluid samples containing the various analyte species are introduced from the top side of the chip, pass through the analysis/reaction chamber, and exit out the bottom region of the assembly. Glass cover slips spaced ~50 μm from the top and bottom of the chip serve to direct the fluids through the various miniaturized analysis/reaction chambers. The top cover slip also serves to confine the beads to their respective wells. The small size of the hole at the bottom of the well prevents the loss of these sensor microspheres through this region of the chip.

available commercially as needed for a variety of solid-state synthetic applications.[63]

The choice of the polystyrene−polyethylene (small molecule, anions, cations) and agarose (enzymes, proteins, antibodies) microspheres for these studies was based, in part, on the good optical transparency of these bead matrixes, the availability of microspheres with diameter values in the range of 120−350 μm, and their compatibility with the solvents of interest.[64] For both types of beads, the microspheres swell in size in a dramatic manner upon their exposure to organic and aqueous fluids. Under typical analysis conditions, ~85% of the internal environment of the microsphere is composed of solvent. A light cross-linking of the matrix backbone provides good mechanical properties to these systems as well as a restoring force that fosters the reversible exchange of solvents in to and out of the microspheres. Immobilizing the polymer beads within cavities in the chips allows for the full advantage of polymer swelling, while avoiding problems incurred by attaching the polymer to a platform. It should be appreciated that with the use of these microporous beads it is possible to utilize an effective sampling thickness of 250−350 μm. This long effective path length combined with large flow rates (vide infra) has the potential to lower detection thresholds and increase measurement sensitivity for the microbead array methods relative to other array strategies that exploit monolayer films or thin polymeric pads.[14]

The sensor array chips are sealed within a customized flow cell designed to minimize exchange volume and allow optical measurements to be made, Figure 2A. The flow cell is essentially composed of two siloxane polymer layers that are held together by a two-piece aluminum casing. Solutions are typically introduced to the flow cell using a liquid chromatography system. Liquid samples can also be introduced into the cell using a syringe via a Luer lock connection. Top and bottom reservoirs are created with thin depressions in the siloxane layers. Source (top) and drain (bottom) layers that service the microbead array are connected to the delivery and exit tubing of the fluid delivery system. Using this type of fluid packaging method alongside liquid chromatography systems, it is possible to acquire rapidly concentration isotherms for a variety of analytes over broad sample ranges. Using the stated top-to-bottom flow direction, the beads become forced to the lower region of the cell and under these circumstances the pyramidal pits serve as self-centering aids, Figure 2B. Fluid flow rates of

(63) *Combinatorial Chemistry Catalog and Solid-Phase Organic Chemistry (SPOC) Handbook*; Novabiochem: Laufelfingen, 1997.

(64) For some of the protein/antibody studies shown in this work, carbonyl diimidazole-activated Trisacryl GF-2000 beads were exploited, which had size diameters of ˜80 μm. For these studies, a specialized Si chip array was used which had a bottom opening of ˜50 × 50 μm.

1−10 mL/min of aqueous samples can be directed through these cells without cell leakage. For small arrays (i.e., 3 × 4 elements), ~30 000 microsphere dead volumes per minute can be forced through each microreactor/analysis chamber.

The flow cell sits atop the base of an optical/fluorescence microscope. The microscope is outfitted with both top and bottom white light illumination as well as with a mercury lamp for fluorescence excitation. Removable filter cubes can be inserted to provide control over the excitation and emission wavelengths. The array is observed and analyzed through the microscope optics using a three-chip CCD. The CCD in conjunction with video capture cards and imaging software can be exploited to analyze the spectral changes. Solution introduction, image capture, and data extraction are completed using a computer controller.

The immobilized beads function as microcuvettes, through which analyte−receptor interactions can be observed optically. Both fluorometric (based on epifluorescence data) and colorimetric (based on transmission data) procedures are used to quantify analyte concentration. In the transmission experiments, colorimetric changes are evaluated using light that passes through the microspheres and the open windows in the microarray. Optical changes in the individual sensing elements are recorded using a remotely spaced CCD detector. In principle, this CCD element can be attached directly to the rear face of the sensor suite as may be the case for future generations of this type of sensor. For current generation studies, a commercial-grade 24-bit video camera is used to detect sensor changes, providing the ability to acquire images at a rate of ~30 frames/s. This speed is valuable in the initial kinetic characterization of microsphere-based sensors. Although not discussed at length here, evaluation of the transient data can provide an additional means to identify the chemical composition of the samples. It should be emphasized that the rapid acquisition of time-dependent colorimetric data provides a particularly powerful analytical capacity when these capabilities are combined with modern pattern recognition algorithms.[18,65−68]

Numerical data can be extracted from the CCD images either in near real time or after the experiment using a stored video. In either case, the user defines an area of interest (AOI) for each bead in the array. The red, green, and blue (RGB) intensities for each AOI can then be automatically exported into a spreadsheet for further manipulation. For colorimetric detection schemes, three "effective absorbance" values are determined (eqs 1−3), using the RGB color intensities of an underivatized

$$A_R \approx -\log\{I_{R,s}/I_{R,0}\} \quad (1)$$

$$A_G \approx -\log\{I_{G,s}/I_{G,0}\} \quad (2)$$

$$A_B \approx -\log\{I_{B,s}/I_{B,0}\} \quad (3)$$

or "blank" bead (i.e., the reference) in coordination with the values taken from an indicator bead (i.e., the sample). Here the A_R, A_G, and A_B variables refer to the effective absorbance values at the three primary color ranges; $I_{R,s}$, $I_{G,s}$, and $I_{B,s}$ define the average raw light intensities for the three colors; and $I_{R,0}$, $I_{G,0}$, and $I_{B,0}$ refer to the average light intensities measured for the reference channels.

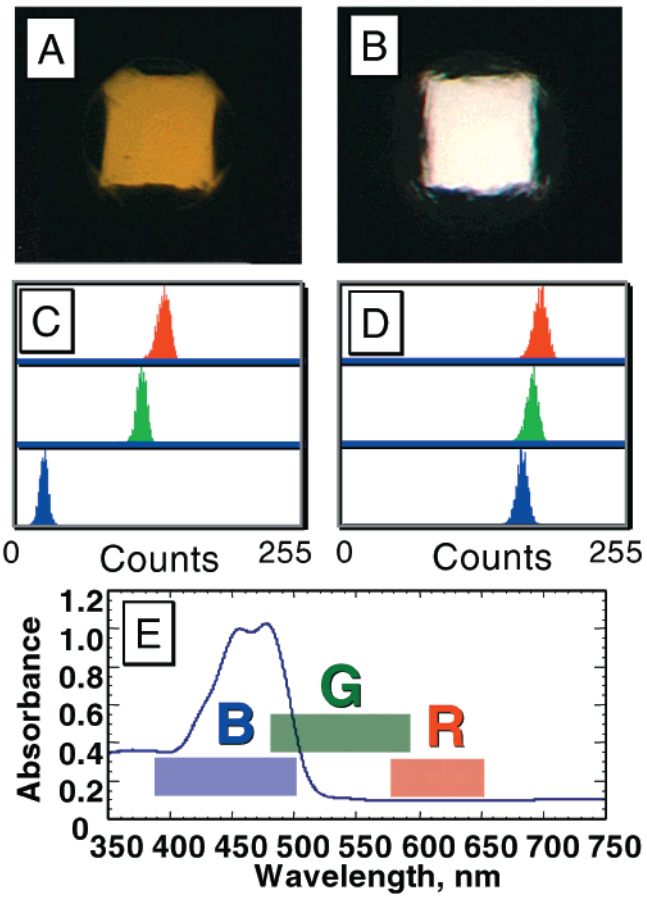

Figure 3. Optical information recorded simultaneously at different cells for use in acquiring crude spectrophometric data. For example, when the array is visualized with transmitted light, the fluorescein-derivatized microsphere shown in panel A displays a yellow hue. The blank microsphere shown in panel B displays a white appearance. The CCD camera located adjacent to chip yields the RGB color intensities as provided by the 200−500 pixel elements that are focused onto each microsphere. The RGB color histograms for the (C) fluorescein-derivatized microsphere and (D) the blank microsphere can be used to quantitate the color attenuation observed in each of these spectral regions. The approximate RGB spectral sensitivity ranges and the absorbance spectrum of the fluorescein dye in solution are provided in panel E. While not as accurate as a conventional spectrophotometer, the array structure can be used to acquire approximate absorbance values for the three broad color ranges at ~100 sites at 30 Hz. In this simple example, the blank bead serves as the reference channel and the dye-coated microsphere serves the role of the sample in analogy to a "double-beam" spectrophotometer.

Figure 3 displays two representative images recorded with transmitted light. One of the images shows a fluorescein-coated bead and the other a blank bead, cases A and B, respectively. Here the images of the beads are focused onto 200−500 pixels. Cases C and D of the illustration provide pixel RGB color intensity histograms for these beads. The absorbance spectrum of fluorescein, included in case E, shows that the dye absorbs light primarily in the wavelength range corresponding to the B channel and to a lesser extent in the G channel of the CCD. Thus, it is possible to quantify crude optical changes and acquire data in an efficient way from multiple reactor sites/analysis chambers. Further, some indicators permit the use of an internal reference for absorbance calculations. The internal reference method can be applied if the signal intensity of the R, G, and B channels is comparable (i.e., following a white balance of the CCD) and if the signaling dye possesses one or more

(65) Osbourn, G. C.; Martinez, R. F. *Pattern Recognit.* **1995**, *28*, 1783−1806.
(66) Hecht, H. G. *Mathematics in Chemistry: An Introduction to Modern Methods*; Prentice Hall: Englewood Cliffs, NJ, 1990.
(67) Gardner, J. *Sens. Actuators, B* **1991**, *4*, 109.
(68) Gardner, J. W.; Shurmer, H. V.; Corcoran, P. *Sens. Actuators, B* **1991**, *4*, 117.

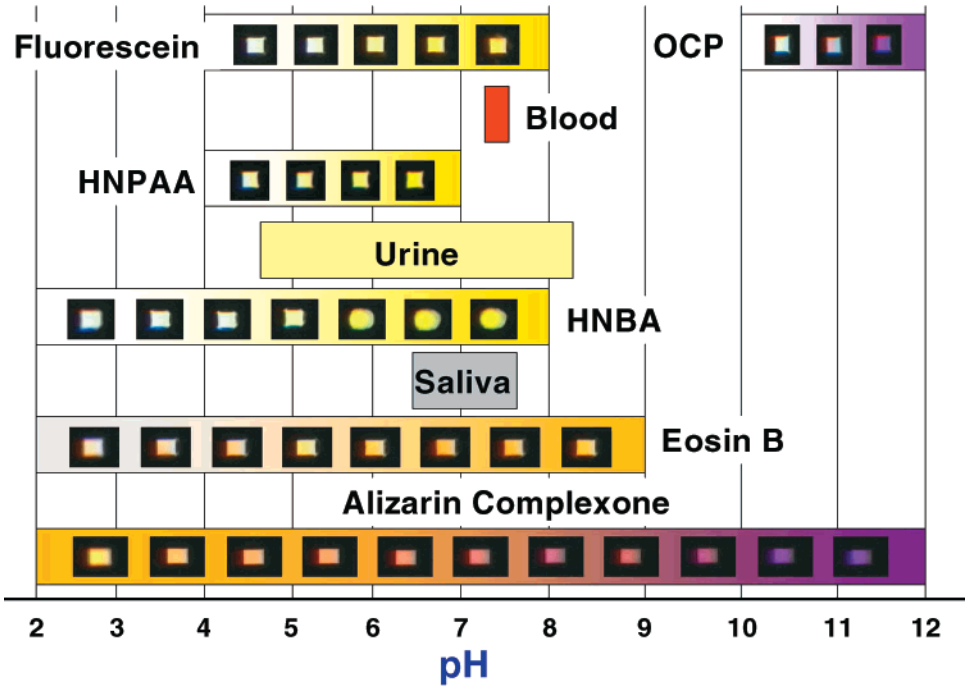

Figure 4. A series of optical micrographs recorded for six strategically chosen indicator dye-coated microspheres. The dyes in each case are anchored covalently onto microsphere resin. Each of these beads is exposed to 10 different solutions with pH values ranging from 2 to 12. The various indicator dyes exhibit a variety of spectral changes that can be used to create unique spectral signatures associated with each of these pH values. These solutions span physiological pH values for a number of common bodily fluids.

transparent channels that remain unchanged throughout the analyte exposure. Here the unaltered channel can be used as an internal reference for the calculation of the effective absorbance values.

With the new instrumentation, reproducibility, reversibility, concentration thresholds, and response times can be measured for both static and flow-based experiments (vide infra). By selecting multiple microspheres from the same batch of beads, it is possible to define the site-to-site variance for identical indicators. Analysis of the optical response properties for individual beads yields a bead-to-bead relative standard deviation (RSD) of only 2−4%. The selection of beads having nearly identical diameter values is an essential variable in defining the site-to-site RSD. These reproducible results suggest that the initial training set of a few selected beads can be used to define the expected optical signatures recorded for beads prepared from the same batch. This important feature will undoubtedly be used in future studies for these microbead arrays.

One of the most powerful attributes of the microbead array detectors is their promise to assay multiple analytes in a rapid manner; however, before such studies are prudent it is necessary to understand the behavior of simple analytes. Therefore, prior to attempting complex multianalyte detection, it is essential to characterize fully the sensor suite in a conceptually simple, single-analyte environment. With this is mind, a series of pH-indicating dyes have been immobilized onto the microspheres. To ensure a broad analytical range, the dye selection is made so that a large range of pK_a values is covered. Although 20 dye candidates are studied in this context, a total of six strategic dyes are selected here for more careful analysis in the context of a customized chip that is optimized for pH detection. These six dyes, along with underivatized blank beads, are used to explore the accuracy and reproducibility of the array for measurement of this standard analyte. Figure 4 shows a series of optical micrographs for these indicator dyes as the pH is varied over the range of 2−12 in one pH unit intervals. With this group of dyes, meaningful color changes are noted over the entire range of proton concentration.

From an analysis of the optical data for these pH indicator-substituted beads using eqs 1−3, a series of bead-based concentration−response curves can be generated. Among the immobilized pH indicators, simple monoprotic dyes have yielded the most sensitive responses. Consequently, many of the initial studies have focused on beads derivatized with 4-hydroxy-3-nitrophenylacetic acid (HNPAA), which displays this feature. Shown in Figure 5A are data obtained for the HNPAA indicator, where two curves for separate HNPAA-coated beads are included. Here nearly identical responses for the two microsphere detectors are obtained. In both cases, the HNPAA-derivatized beads remain transparent below a pH of ∼4. At higher pH values, a strong attenuation of the transmitted light in the B channel is observed. Little absorbance is noted in the R and G channels for the same dye over the entire range of examined pH values. The most dramatic changes in the B channel are observed near a pH of ∼6 and the full color develops at pH values of >8. Above pH 8, the color attenuation remains constant.

While immobilization of the indicator may cause a shift in pK_a, the shapes of the two experimental curves are in excellent agreement with that of a hypothetical solution titration curve (plotted for pK_a = 6.25). It should be noted that this indicator dye provides useful proton concentration information only over 2−3 decades of concentration. The dynamic range for proton detection, however, can be expanded through an analysis of the optical properties of the other members of the array. Alternatively, it is also worth noting that in applications which do not require sensitive pH measurements, a single bead type having an indicator with multiple ionizable protons (such as alizarin complexone) can provide sufficient information concerning pH over a broad range of acidities. Thus, an important concept is demonstrated here. That is, through the judicious choice of multiple receptors having variable binding affinities, it is

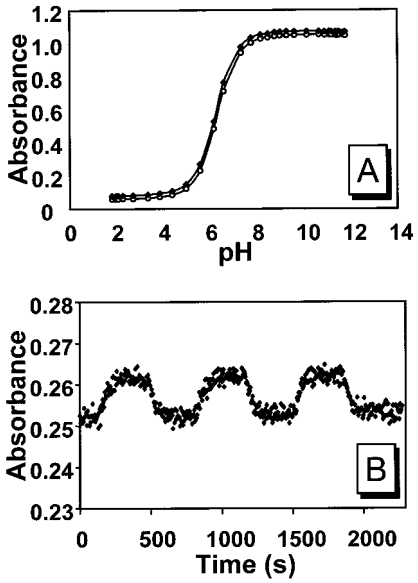

Figure 5. (A) Effective absorbance values in the blue range plotted for two HNPAA-coated microspheres as a function of solution pH. (B) To demonstrate the pH sensitivity of the absorbance detection method, the time evolution of the blue "effective" absorbance values for the same HNPAA system are plotted as a function of time as buffer solutions of pH 6.00 and 6.05 are swept through the array structure at regular time intervals. Absorbance values of ~0.25 are acquired when the pH 6.00 buffer bathes the microspheres, and this increases to ~0.26 upon replacement with the pH 6.05 buffer solution.

possible to extend the useful analytical detection range of the array. Under ideal cases where simple equilibria are established, a single indicator type is able to service concentration ranges that span factors of 100−1000. A preliminary neural net analysis of a series of 12 beads (i.e., the same 6 beads described above with a 2-fold redundancy factor) has been completed. Here comparisons are made between the values measured with a calibrated standard glass electrode and those values extracted from a neural net analysis. Quite interestingly, even at this initial stage the agreement between the two methods is excellent (~0.02 pH unit variance). Future reports will provide more extensive discussion of the important details related to exploitation of the pattern recognition to the microbead array analyte classification, identification, and quantitation issues.

Figure 5B shows the B channel absorbance changes as the pH of the analysis fluid is altered from 6.00 to 6.05. Absorbance values are shown here for the B channel only, using the R channel as the reference intensity (as described above). Even these modest alterations in proton concentration evoke meaningful changes that are easily measured by the sensor array. Analysis of the optical response curves for a single bead reveals that the detection limit for the HNPAA bead is less than 0.05 pH unit. Interestingly, when the absorbance values for 12 beads are averaged, the standard deviation of the array's responses (both at 6.00 and 6.05) are found to be <0.001 au, corresponding to a detection threshold of ≤0.01 pH unit. Collectively, these results suggest that the sensor array technology herein described can yield impressive analytical data, comparable to that achieved by commercially available pH meters. However, unlike conventional glass electrode pH meters, calibration may not be necessary following the initial training of the array.

A 4 × 3 array populated at each cell with HNPAA microspheres is prepared as illustrated in Figure 6 to demonstrate the site-to-site reproducibility, the uniformity of the fluid delivery, the dynamic microarray response under flow conditions, and the microsphere response times. In the left panel is shown a photomicrograph of the array recorded under flow conditions (at 2 mL/min). The self-centering feature of the pyramidal pits described above is evident here as all the beads remain stationary at the bottom of the wells during the entire duration of the experiment. Included in the same illustration in the right panel is the temporal responses acquired in the B color range for each of the 12 microspheres as pH 5.00 and pH 8.00 buffer solutions flow twice through the array. Not only is the pH response within each individual bead reproducible, there also seems to be little difference in the timing of the responses across the array. While these initial results are promising, it will be useful to perform similar studies in the future with larger arrays and with a wide range of analytes, especially those with large molecular weights. Choice of high-affinity receptors may also alter the observed signal uniformity at the various sites. Flow-based studies that alter these variables in systematic ways are currently in progress.

To expand the chemical diversity of the microbead array, attention has been directed to the area of metal cation sensing. As an initial example, an established complexiметric indicator, *o*-cresolphthalein complexone (OCPC), is used in a colorimetric scheme for detection of Ca^{2+}. This indicator molecule undergoes a dramatic optical change from clear to deep purple upon its deprotonation at pH values of ~11. The presence of Ca^{2+}, however, lowers the pH at which this optical change occurs. Likewise, if the solution pH is lowered to the range of 9−10, the OCPC-beads' spectral features can then be used to measure Ca^{2+} concentration. Indeed, in this context, the OCPC system is well-suited for use in determinations of water hardness where typical concentrations of Ca^{2+} ranges from 0.10 to 3.0 mM[69] and human blood serum Ca^{2+} where a range of 2.15−2.57 mM is commonly observed.[70] In both cases, the detection threshold for the discussed common Ca^{2+} assays falls below the minimum values needed for these analyses, thus allowing for the dilution of sample media.

Initial work using OCPC-derivatized microspheres to detect Ca^{2+} is performed using a stopped-flow method. Here ~100 μL (i.e., 2 drops) of the test solution is introduced into the array, and then further sample introduction is terminated. After an equilibration time of 1 min, the data are acquired. Figure 7 shows a plot of green absorbance vs Ca^{2+} concentration for a single OCPC-derivatized bead. These data establish a linear calibration curve over a concentration range that spans ~2 orders of magnitude. Studies of this type also demonstrate that the microbead assays can be used in conjunction with Beer's law to measure solution dissolved analyte concentration values. Interestingly, other studies (not shown here) attest to the fact that with the use of flow-based experiments analyte sequestration behavior can be noted. As a demonstration of this capability, a 3 × 4 array composed of OCPC-derivatized and blank microspheres is considered. This 12-element array is subjected to continuous-flow conditions with a rate of 2 mL/min. Here various solutions containing different amounts of dissolved Ca^{2+} are sampled through the array. Under these rapid-flow conditions, the green absorbance values are found to increase with time initially in a linear manner. Eventually signal saturation is observed (see Supporting Information). When the internal bead volume of ~ 5 nL is combined with the utilized flow rate, an effective sampling volume corresponding to ~30 000 dead volumes delivered to each bead compartment/min is obtained. While only a small fraction of the analyte permeates the beads under these conditions, the large fluid handling capabilities exhibited by these microbead arrays would seem to make these

(69) Yappert, C. M.; DuPre, D. B. *J. Chem. Educ.* **1997**, *74*, 1422.
(70) Burtis, C. A., Ashwood, E. R., Eds. *Tietz Textbook of Clinical Chemistry*, 2nd ed.; W. B. Saunders Co.: Philadelphia, 1994.

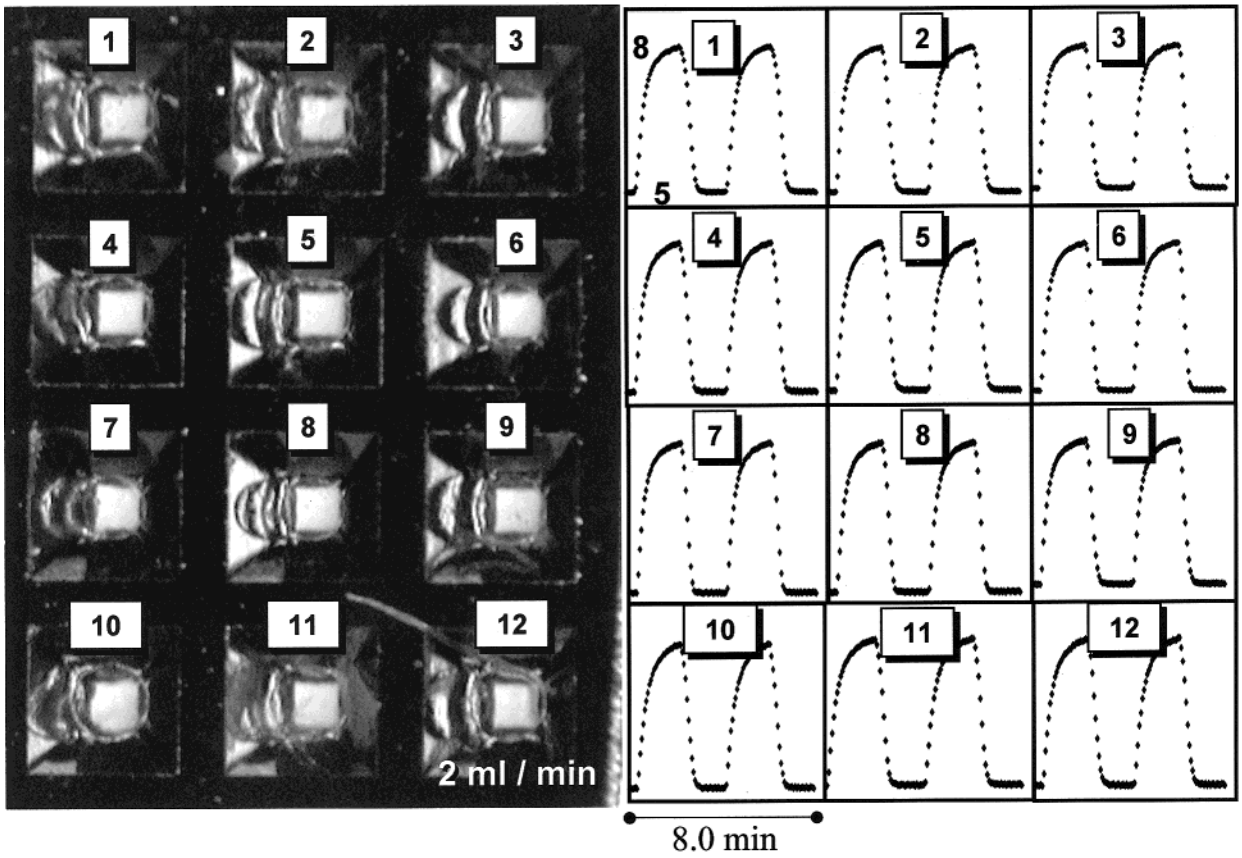

Figure 6. A 4 × 3 array composed of HNPAA microspheres demonstrating the site-to-site reproducibility, the uniformity of the fluid delivery, and the microsphere response times. At the left is shown a photomicrograph recorded with a combination of top and bottom illumination for this microbead array. At the right is plotted the temporal response acquired in the blue color range for each of the 12 microspheres as pH 5.00 (low absorbance response) and pH 8.00 (high absorbance response) buffer solutions flow twice through the array.

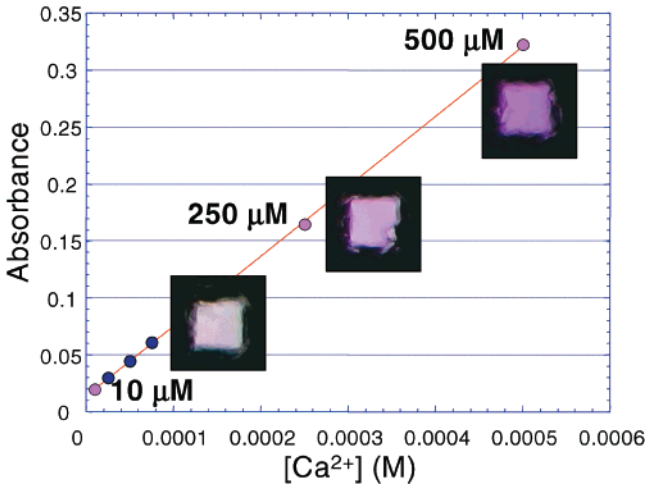

Figure 7. Green effective absorbance vs Ca^{2+} concentration calibration plot for a single OCP-coated microsphere over the concentration range of 10−500 μM. The data here are acquired with a stopped-flow method whereby 2 drops of the analysis fluid is introduced into the chip in each case.

systems quite suitable for trace analyses. Indeed, using the flow method, the useful range of Ca^{2+} detection with OCPC can be extended an additional 2 orders of magnitude (lowering the Ca^{2+} detection threshold from 10 μM to 100 nM). Furthermore, the use of large sample volumes also allows for the completion of thorough rinsing of the beads following the completion of the experiments. In the case of Ca^{2+} detection with OCPC-beads, the microspheres can be refreshed and returned to the original Ca^{2+} detection free form simply by rinsing with various buffers and/or EDTA solutions (see Supporting Information). Washes over a period of 8−10 min can be used to regenerate signals to within 2−3% of the original values. As with the pH experiments mentioned above, reversible detection for Ca^{2+} is observed with the use of the OCPC-beads.

A large expansion in the number of metal cations that can be detected by the microbead array becomes feasible with the attachment of a few more strategically chosen complexometric indicators onto the microspheres. A series of promising indicator systems of this type have been identified and studied in this context. Figure 8 demonstrates the capability of an array to sense and distinguish three very similar metal cations. The array contains six different types of beads (five complexones and one blank, each expressed with 2-fold redundancy), which are summarized in Table 1. Each panel of the figure contains a series of bar graphs which define the measured RGB absorbance values for the five different complexone beads in a given solution environment. The four solutions corresponding to the various panels are as follows: (A) pH 9.8; (B) 10 mM $MgCl_2$ at pH 9.8; (C) 10 mM $Ca(NO_3)_2$ at pH 9.8; (D) 10 mM $BaCl_2$ at pH 9.8. To acquire such measurements, solutions are delivered through the array for 12 min at 2 mL/min, ensuring thorough analyte exposure. Accompanying each graph is a photomicrograph of the array from which the displayed data are extracted. To facilitate the analysis, pairs of identical beads have been grouped together with colored code boxes.

While two of the bead types, OCPC (red box) and calcon-carboxylic acid (Kalces, green box), appear to yield unique responses for each of the four environments, the others such as thymolphthalexon (ThyPh, blue box) respond to several cations more or less indiscriminately (Ca^{2+} and Mg^{2+}, in this case).

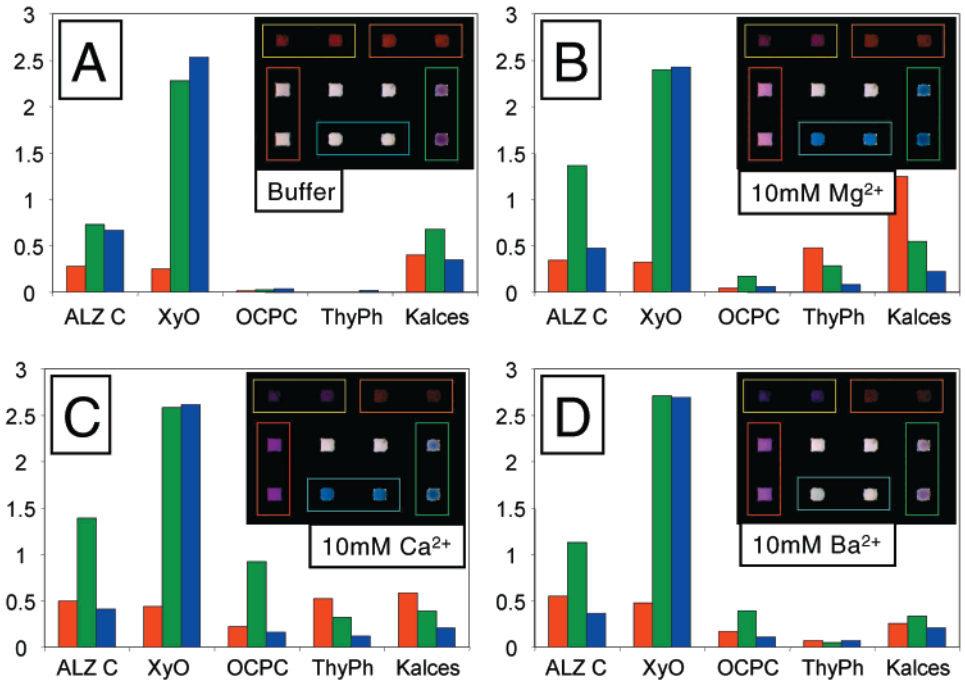

Figure 8. Red, green, and blue absorbance values for a series of complexometric dyes as obtained in four different environments: (A) pH 9.8 buffer; (B) pH 9.8 buffer, 10 mM $MgCl_2$; (C) pH 9.8 buffer, 10 mM $Ca(NO_3)_2$; (D) pH 9.8 buffer, 10 mM $BaCl_2$. The inset on each graph is an optical micrograph of the array from which the data have been extracted. Table 1 provides a summary of the various indicator dye systems used here as well as their locations within the array.

Table 1. Summary of Compleximetrix Dyes and Associated Analytes

indicator molecule(s)	location (row, column)	detection method	known analytes[a]	pH-sensitive range	ref
alizarin complexone (ALZ C)	(1,1), (1,2)	abs	La^{3+}, Ce^{3+}, Zr^{4+}	~2−12	78
xylenol orange (XyO)	(1,3), (1,4)	abs	Al^{3+}, Bi^{2+}, Cd^{2+}, Ce^{3+}, Cr^{3+}, Dy^{3+}, Fe^{3+}, Ga^{3+}, Gd^{3+}, Hf^{4+}, Hg^{2+}, In^{3+}, La^{3+}, Mn^{2+}, Mo^{6+}, Nb^{5+}, Nd^{3+}, Ni^{2+}, Pb^{2+}, Ru^{3+}, Sc^{3+}, Sm^{3+}, Sn^{4+}, Th^{4+}, Ti^{3+}, Tl^{3+}, U^{4+}, U^{6+}, V^{4+}, V^{5+}, Y^{3+}, Yb^{3+}, Zn^{2+}, Zr^{4+}	~6−8	78, 79
o-cresolphthalein complexone (OCPC)	(2,1), (3,1)	abs	Ba^{2+}, Ca^{2+}, Mg^{2+}, Mo^{6+}	~10−12	78, 79
thymolphthalexon (ThyPh)	(3,2), (3,3)	abs	Ba^{2+}, Ca^{2+}, Mg^{2+}, Nd^{3+}, Pr^{3+}, Sm^{3+}, Yb^{3+}, Sr^{2+}, Mo^{6+}	~8−10	79
calconcarboxylic acid (Kalces)	(2,4), (3,4)	abs	Ca^{2+}, U^{6+}	~10	78, 79
acetylated resin (blank)	(2,2), (2,3)	abs	none	~2−12	79

[a] Known analytes based on indicator uses reported within referenced literature.

Furthermore, the xylenol orange beads (XyO, orange box) respond to the presence of all three cations, but fail to provide a species-specific response. An important conclusion derived from this study is that while individual beads may be incapable of distinguishing among these cations, the data extracted from multiple bead types can be used to generate optical fingerprints that are unique for the each cation. The panels in Figure 8 represent four such fingerprints. The ability to generate such unique spectral signatures even for a series of chemically similar species (i.e., all group 2 divalent cations) bodes well for the future expansion of this methodology to other more chemically distinct regions of the periodic table. Furthermore, a collection of these fingerprints can be used to train pattern recognition algorithms for analyte recognition and quantification. The implementation of such pattern recognition techniques will be an essential part of multianalyte sensing as the complexity of the analyte mixtures and the number of elements within arrays increase.

A further extension of the array's capabilities is now considered in the context of enzyme-based assays. Indeed, a large number of prior studies have shown enzymes to be useful for the quantitation of biologically relevant analytes.[71] Enzymatic glucose sensors, for example, have been developed to sense for glucose content through a number of detection schemes.[72,73] A frequent mode of detection is to utilize the properties of a product of the enzymatic reaction. In the case of dehydrogenases, this can include evaluations of the production of NADH fluorescence.[74] Alternatively, amperometric determination of hydrogen peroxide produced by the action of an oxidase has

(71) Winartasaputra, H.; Mallet, V.; Kuan, S.; Guibault, G. *Clin. Chem.* **1980**, *26*, 613−617.
(72) Appelqvist, R.; Marko-Varga, G.; Gorton, L.; Torstensson, A.; Johansson, G. *Anal. Chim. Acta* **1985**, *169*, 237−247.
(73) Curey, T. E.; Goodey, A. P.; Tsao, A. S.; Lavigne, J. J.; McDevitt, J. T.; Anslyn, E. V.; Neikirk, D.; Shear, J. B. *Anal. Biochem.*, submitted.
(74) Rangel, A.; Toth, I. *Anal. Chim. Acta* **2000**, *416*, 205−210.

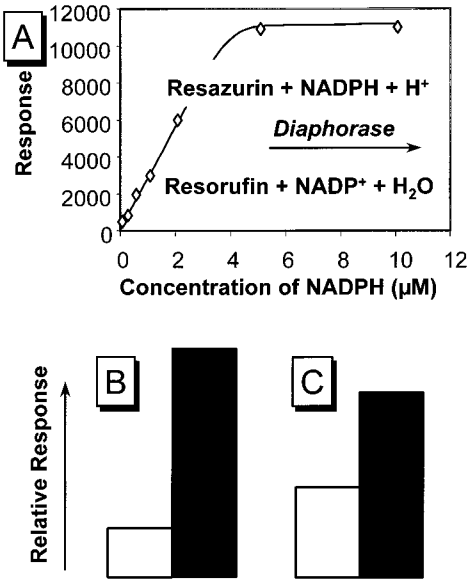

Figure 9. (A) Calibration plot showing the working range for the diaphorase-catalyzed reduction of resazurin to resorufin. The response of the assay is linear to ~2 μM NADPH and saturated at concentrations above 5 μM. (B, C) The enzymatic rate of catalysis (black bars) drops with an increase in reaction pH of 7.0 (B) to 7.5 (C), while the absorbance of an HNPAA (white bars) bead increases with the same pH change. A bead derivatized with HNPAA is capable of evaluating pH in the physiologically relevant range of 6−8. Therefore, in an array containing both types of beads, the HNPAA bead can be used to calibrate the response of diaphorase.

been demonstrated.[75] In most cases, however, the sensing scheme is designed to assay for one component only, whereas blood or other clinically relevant samples contain a large variety of components, some of which may actually interfere with the accurate determination of another component.

Likewise, new opportunities exist now for the measurement of a number of analytes using simultaneous enzyme assays.[14,76] The inclusion of enzyme assays into a microarray format allows for the detection of different analytes at various locations thereby allowing, for example, the simultaneous detection of glucose and proton content.[73] As a demonstration of microbead array enzyme assays described here is the NADPH determination. The analysis proceeds through the oxidation of NADPH and reduction of resazurin catalyzed by the enzyme diaphorase as shown in Figure 9A. The resulting resorufin is strongly fluorescent, and its production can be monitored using the R channel of the CCD (excitation maximum at 560 nm, emission maximum at 584 nm). In addition to NADPH detection, diaphorase also recognizes NADH. Both NADPH and NADH are produced by the action of a number of dehydrogenases such as glucose, carnitine, and cholesterol dehydrogenase. Any dehydrogenase that catalyzes the reduction of either cofactor can be used in conjunction with the diaphorase scheme to determine the concentration of the substrate of interest.

In contrast to the above-described analyses where the instantaneous color attenuation properties are correlated with identity and concentration of analytes, in the case of the described enzyme assay, fluorescence intensity develops with time as the fluorophore collects within the microreactor region. The concentration of the analyte is evaluated from the initial velocity of the reaction (defined as the first derivative of the initial portion of the development of fluorescence). This value is plotted against NADPH concentration and produces a calibration curve, shown in Figure 9A, demonstrating that the assay is linear with concentration up to ~2 μM NADPH. The bead-localized enzyme appears to become completely saturated above ~5 μM.

Enzymes are known to be strongly affected by their solution environment including ionic strength, presence of inhibitors, temperature, and pH. As a further example of the strength of array format measurements, the response of diaphorase is evaluated for a single concentration of NADPH at two different pH values, Figure 9B,C. The enzymatic response of diaphorase drops in going from a reaction pH of 7.0 to 7.5. Within the same array are included beads derivatized with HNPAA which experience an increase in absorbance as the proton concentration is altered in this way. Indeed, the optical response of the pH-sensitive bead can be used to interpret the signal of the enzyme bead.[73]

As a final example of the utility of the microbead array sensors, the method is extended to the study of immunological interaction wherein the detection of viral agents is demonstrated. Many current viral antibody screening tests rely upon enzyme-linked immunosorbant assay (ELISA) techniques to detect the presence of antibody in human blood serum.[77] In these techniques, the wells of a microtiter plate are coated with a specific viral antigen. Diluted human blood serum is added to the wells and allowed to incubate or interact with the coated wells. Then the wells are rinsed to remove any unbound reagents. If the antibody of interest (antigen-specific IgG or IgM) is present, it will bind to the antigen via specific hydrophobic/hydrophilic and electrostatic charge interactions. The presence of this antibody/antigen complex is detected by the addition of an IgG/IgM specific secondary antibody conjugated to an enzyme (i.e., horseradish peroxidase or alkaline phosphatase). Upon the addition of a soluble substrate, the enzyme will then catalyze a reaction to produce a chromophore whose absorbance is measured using standard spectrophotometric techniques.

Conforming to the principles of such immunological assay techniques outlined above, methods have now been developed and optimized that allow for specific viral antigens to be covalently linked to the polymer microsphere supports. Figure 10A,B shows a schematic of a bead-based immunoassay. Multiple immunoassays can be performed simultaneously when an array of "antigenic beads" is placed in the wells of the silicon chip. Figure 10C demonstrates that good immunoselectivity is observed when triplicate trials of three different antigenic bead types (HIV gp41/120, Flu A, and HBsAg) are tested for signal intensity, cross-reactivity, and nonspecific binding of protein. In this experiment, HBsAg-specific IgG is diluted to physiologically relevant concentrations and allowed to incubate with the bead array using the fluid flow techniques described above. Unbound HBsAg IgG is then washed away using Tris-buffered saline, pH 7.6. A solution of secondary antibody conjugated with the fluorophore, Cy2[51] is then allowed to incubate over the bead array. Upon washing away unbound secondary antibody, evaluation of a captured image reveals the average signal intensity of the HBsAg beads is significantly greater than that of the negative controls. These data enable further research in applying this bead array methodology for use in multianalyte

(75) Perdomo, J.; Sundermeier, C.; Hinkers, H.; Morell, O. M.; Seifert, W.; Knoll, M. *Biosens. Bioelectron.* **1999**, *14*, 27−32.
(76) Healey, B. G.; Li, L.; Walt, D. R. *Biosens. Bioelectron.* **1997**, *12*, 521−529.
(77) Hornbeck, P. In *Current Protocols in Immunology*; Coligan, J. E., Kruisbeek, A. M., Margulies, D. H., Shevach, E. M., Strober, W., Eds.; John Wiley and Sons: New York, 1998; Chapter 2, Section 1.
(78) Green, F. J. *The Sigma-Aldrich Handbook of Stains, Dyes and Indicators*; Aldrich Chemical Co., Inc.: Miwaukee, WI, 1990.
(79) Hulanicki, A.; Glab, S.; Ackerman, G. *Pure Appl. Chem.* **1983**, *55*, 1137−1230.

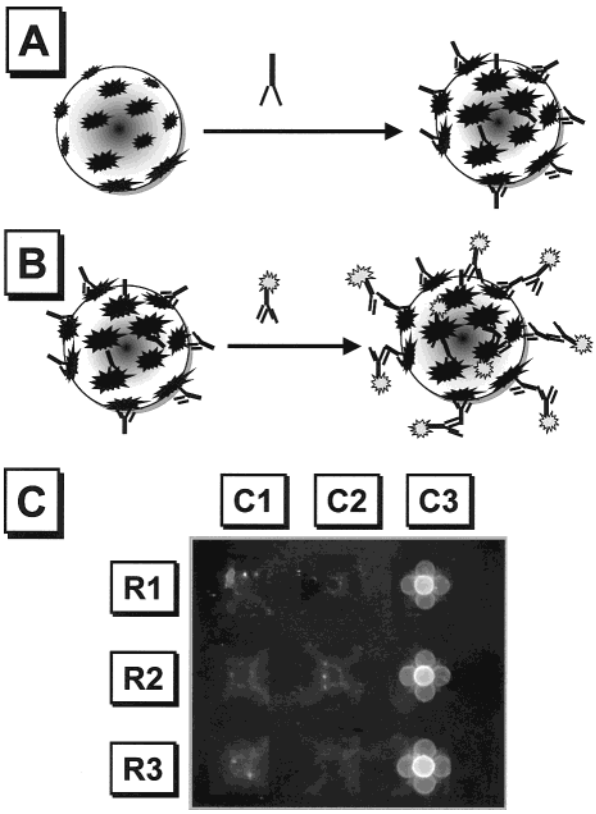

Figure 10. Schematic diagrams depicting the basic steps involved in the sequestration and sensing of solution-dissolved antibody species. (A) In the initial stages, the viral antigens that are bound to the specific beads are exposed to the sample fluid that may contain the antibodies of interest. If the specific target antibodies are present, the formation of a bead-localized antibody−antigen complex can occur. (B) In the subsequent step, a visualization process is completed whereby the bead-localized complexes are exposed to a fluorophore-conjugated secondary antibody which can bind to the common regions of the sequestered antibodies. Following a wash step to remove unbound visualization reagents, the fluorescence pattern observed over the array can be used to identify the presence or absence of a series of specific antibodies. (C) To demonstrate the functionality of such a chip-based multiplexed antibody test, an array is assembled having the following three antigens anchored to microspheres: HIV gp41/120 in column 1 (C1), influenza A in column 2 (C2), and hepatitis B surface antigen (HBsAg) in column 3 (C3). Within the array, three identical beads are included within each row allowing for the data sets to be acquired in triplicate for each of the represented antigens. The nine-element array is exposed to a small amount of fluid containing the monoclonal antibody to HBsAg and allowed to incubate. In subsequent steps, reaction with fluorophore-conjugated goat anti-mouse antibody followed by washing reveals good immunoselectivity with little cross-reaction and nonspecific binding.

diagnostic testing. A variety of customized viral chips can be envisioned following the successful demonstration here reported.

Conclusion

In summary, the covalent derivatization of microspheres with strategically chosen colorimetric indicators, enzymes, and biological proteins has been completed to create a variety of structures that exhibit sensitivity to important and interesting analytes. With the appropriate choice of a microporous bead, these structures can be combined with micromachined silicon wafers to generate novel microbead array sensors. These derivatized microspheres can be prepared in a highly parallel manner (10^6 beads/g) using standard solid-state synthetic methods. This feature combined with the use of standard lithographic procedures capable of fabricating a large number of microarrays suggests that this sensor methodology may find utility for a number of interesting applications wherein inexpensive/disposable sensor elements are needed.

The beads localized within pyramidal pits of patterned Si wafers can serve both as microreactors and as miniaturized analysis chambers. When interfaced with a CCD camera, fluid delivery system, and a video capture card, these microbead arrays can serve as the heart of a powerful new chip-based total analysis system. The concept for such an analysis system has been described in this paper along with initial experiments that demonstrate its utility for a broad class of analytes. With this new instrumentation, the following important accomplishments have been demonstrated to date: (1) near-simultaneous collection of absorbance or fluorescence signals at multiple sites, (2) production of polymer bead-based chemical sensor array with site-to-site optical response variance of 2−4%, (3) detection of pH over 10 decades of proton concentration with agreement to within ±0.02 pH unit of that acquired at glass electrodes, (4) reasonably rapid array data acquisition rate of 30 Hz and typical sensor equilibration times of 2 min, (5) fully reversible detection characteristics (demonstrated here for proton and cations), (6) uniform flow characteristics with little noticeable motion of the microspheres, (7) the ability to pass a large number of dead volumes through the microbead array leading to the significant lowering of the detection threshold, (8) incorporation of receptors/signaling agents suitable for the analysis of acids, bases, numerous metal cations, enzymatic substrates, proteins, and antibodies, and (9) acquisition in near-real-time of data that can be used to interpret the chemical/biochemical content of complex fluids.

The microbead array sensor methodology is extremely versatile. The basic platform can be adapted relatively quickly to a number of "customized" applications. In progress now are "theme" chips for viral agents, bacterial chips, DNA detection, redox-active compounds, disaccharides, anionic species, and solvents. At some level, this microbead array total analysis system can be thought of as a "programmable taste chip". The utilization of the microbead sensor array platform for other application areas requires that new receptors and signaling agents be attached to the microspheres. This task is analogous somewhat to the development of new software modules that can be used on an existing computer platform. Indeed, it is the ability of these microbead arrays to generate digital fingerprints of complex fluids in near-real-time that provides this type of detection methodology promise for future interesting applications including the following: environmental testing, chemical/petrochemical processing, diagnostic testing, medical applications, wine/beer industries, artificial flavor, food industries, health/safety, toxicology monitoring, and waste monitoring.

Acknowledgment. We gratefully acknowledge Dr. Damon Borich, Dr. Carole Moncman, Dr. Annette Soble (M.D.), Dr. Gordon Osbourn, Dr. Steven A. Young, Prof. Brent Iverson, Prof. Al Bard, and Prof. Andrew Ellington for helpful discussions. Funding for this project was provided by the National Institutes of Health, the National Science Foundation (IGERT program), the Beckman Foundation, the Army Research Office (MURI program), the Texas Materials Institute, and the Institute for Cellular and Molecular Biology (UT Austin).

Supporting Information Available: Additional information related to analyte sequestation during extended flow and reversible Ca^{2+} experiments. This material is available free of charge via the Internet at http://pubs.acs.org.

JA003341L